The 2015 Chileno Valley glacial lake outburst flood, Patagonia

Wilson, R., Harrison, S., Reynolds, J., Hubbard, A., Glasser, N. F., Wündrich, O., Iribarren Anacona, P., Mao, L. and Shannon, S. ORCID: https://orcid.org/0000-0002-7644-2724
(2019) The 2015 Chileno Valley glacial lake outburst flood, Patagonia. Geomorphology, 332. pp. 51-65. ISSN 0169-555X doi: 10.1016/j.geomorph.2019.01.015 Available at https://centaur.reading.ac.uk/125275/

Geomorphology 332 (2019) 51–65

Contents lists available at ScienceDirect

Geomorphology

journal homepage: www.elsevier.com/locate/geomorph

The 2015 Chileno Valley glacial lake outburst flood, Patagonia

R. Wilson [a,*], S. Harrison [b], J. Reynolds [c], A. Hubbard [d], N.F. Glasser [d], O. Wündrich [e], P. Iribarren Anacona [f], L. Mao [g,h], S. Shannon [i]

[a] Department of Biological and Geographical Sciences, University of Huddersfield, Huddersfield, UK
[b] College of Life and Environmental Sciences, University of Exeter, Exeter, Devon, UK
[c] Reynolds International Ltd, Broncoed House, Broncoed Business Park, Mold, UK
[d] Department of Geography and Earth Sciences, Aberystwyth University, Ceredigion, UK
[e] Colibri Ventura, Coyhaique, Chile
[f] Faculty of Sciences, Institute of Sciences, Physics and Mathematics, Universidad Austral de Chile, Valdivia, Chile
[g] Estación Patagonia de Investigaciones Interdisciplinarias UC, Instituto de Geografía, Pontificia Universidad Católica de Chile, Chile
[h] School of Geography, University of Lincoln, Lincoln, UK
[i] School of Geographical Sciences, University of Bristol, Bristol, UK

ARTICLE INFO

Article history:
Received 19 September 2018
Received in revised form 17 January 2019
Accepted 17 January 2019
Available online 8 February 2019

Keywords:
GLOF
Glacial lake
Paraglacial response
Patagonia

ABSTRACT

Glacial Lake Outburst Floods (GLOFs) have become increasingly common over the past century in response to climate change, posing risks for human activities in many mountain regions. In this paper we document and reconstruct the sequence of events and impact of a large GLOF that took place in December 2015 in the Chileno Valley, Patagonia. Hydrograph data suggests that the flood continued for around eight days with an estimated total discharge of 105.6×10^6 m^3 of water. The sequence of events was as follows: (1) A large debris flow entered the lake from two steep and largely non-vegetated mountain gullies located northeast of the Chileno Glacier terminus. (2) Water displaced in the lake by the debris flow increased the discharge through the Chileno Lake outflow. (3) Lake and moraine sediments were eroded by the flood. (4) Eroded sediments were redistributed downstream by the GLOF. The post-GLOF channel at the lake outlet widened in some places by >130 m and the surface elevation of the terrain lowered by a maximum of 38.8 ± 1.5 m. Farther downstream, large amounts of entrained sediment were deposited at the head of an alluvial plain and these sediments produced an ~340 m wide fan with an average increase in surface elevation over the pre-GLOF surface of 4.6 ± 1.5 m. We estimate that around 3.5 million m^3 of material was eroded from the flood-affected area whilst over 0.5 million m^3 of material was deposited in the downstream GLOF fan. The large debris flow that triggered the GLOF was probably a paraglacial response to glacier recession from its Little Ice Age limits. We suggest that GLOFs will continue to occur in these settings in the future as glaciers further recede in response to global warming and produce potentially unstable lakes. Detailed studies of GLOF events are currently limited in Patagonia and the information presented here will therefore help to inform future glacial hazard assessments in this region.

1. Introduction

In response to climate change, many hazards associated with glacierised environments, such as ice/rock avalanches, landslides, debris flows and glacial lake outburst floods (GLOFs), have increased in prevalence over the past century, posing risks for human activities in mountain regions (Gruber and Haeberli, 2007; Keiler et al., 2010; Carrivick and Tweed, 2016). GLOFs are particularly significant as they have the potential to impact areas tens to hundreds of kilometers downstream of their source (Richardson and Reynolds, 2000; UNEP, 2007). GLOFs are typically generated either by the failure of ice-dammed or moraine-dammed lakes, the latter forming between the frontal positions of receding glaciers and the terminal moraine ridges that mark the maximum extent of previous advances (typically at the end of the Little Ice Age (LIA) *c.* 1850). As a consequence of the general recession and thinning of glaciers since then, the number and water volume of glacial lakes have increased in many high mountainous regions around the world resulting in an increase likelihood of GLOF events (Paul et al., 2007; Loriaux and Casassa, 2013; Nie et al., 2013, 2017, 2018; Carrivick and Quincey, 2014; Wang et al., 2014; Wilson et al., 2018). High-magnitude GLOFs, involving large volumes of water, have considerable erosion and transport potentials and can deposit large amounts of debris (Clague and Evans, 2000; Breien et al., 2008; Westoby et al., 2014a). Consequently, GLOFs have the potential to significantly alter downstream river channels, destroy valuable agricultural land and

* Corresponding author.
E-mail address: r.wilson2@hud.ac.uk (R. Wilson).

https://doi.org/10.1016/j.geomorph.2019.01.015

infrastructure and impact downstream settlements, in some instances leading to human fatalities (Carey, 2005; Kääb et al., 2005; Huss et al., 2007; Carrivick and Tweed, 2016; Harrison et al., 2018).

GLOFs are initiated by the occurrence of triggering mechanisms and/or the exceedance of dam failure thresholds. The most common triggering mechanism for moraine-dammed lake failures is overtopping, whereby waves produced by mass movements (e.g., snow and debris avalanches) or ice calving events breach the crest of a dam resulting in a progressive failure of the moraine structure (Clague and Evans, 2000; Huggel et al., 2004; Emmer and Cochachin, 2013; Rounce et al., 2016). Structural failure of moraine dams, however, is not necessarily a prerequisite of all proglacial outburst floods. Seiche waves, for example, generated when large mass movements enter lakes with particular bowl-shaped bed geometries, can obtain trajectory heights large enough to travel over impounding moraines leaving their structure mainly intact (e.g., Hubbard et al., 2005). Other GLOF triggering mechanisms include moraine collapse as a result of seismic activity, outflow channel blockage by icebergs, water displacement through the flotation of submerged dead ice, water seepage and piping and the degradation of ice-cored moraines and permafrost as a result of atmospheric warming (Richardson and Reynolds, 2000; Westoby et al., 2014b). The susceptibility of moraine dams to failure is also influenced by threshold parameters such as the effective volume of lake water available for flood, dam freeboard height relative to lake level, the width/height ratio of the terminal moraine dam and the distal gradient of the dam structure (Reynolds, 2014).

In South America, interest in GLOFs has been largely focused on the Peruvian Andes where large outburst events have been directly responsible for >10,000 deaths (Reynolds, 1992; Carrivick and Tweed, 2016). However, the largest concentrations of glacial lakes in this region are located in the Patagonian Andes (36°S–55°S) (Iribarren Anacona et al., 2015a; Wilson et al., 2018). Here, an accelerated rate of glacial retreat over recent decades has resulted in a large increase in both the number and area of moraine- and ice-dammed lakes (Davies and Glasser, 2012; Loriaux and Casassa, 2013; Paul and Mölg, 2014). Such changes have coincided with a possible increase in the frequency of GLOF events, particularly since the 1980s (Iribarren Anacona et al., 2015a). Overall, at least 17 moraine dam failures have been reported in Patagonia since the 1940s, although the actual total is likely to be larger due to under-reporting (Iribarren Anacona et al., 2014; Wilson et al., 2018). Despite occurring in remote mountain basins, the presence of extensive riverine damage (in some instances stretching ~27 km downstream) indicates the involvement of high-magnitude outburst events and, to date, Patagonian GLOFs have been directly responsible for the destruction of houses, the re-location of a village, damage of transport and tourist infrastructure and the loss of three lives (Iribarren Anacona et al., 2014, 2015a).

Whilst continuing to pose a threat to downstream areas, knowledge gaps currently exist in regards to the processes that lead to the generation of GLOFs in Patagonia and there are few studies of their characteristics and geomorphic impacts. Trigger mechanisms, for example, have only been reported for three moraine-dam failures that have occurred at Calafate Lake in the Río Los Leones Valley – triggered by a large rock-fall (Harrison et al., 2006), in the Río Engaño Valley – dam breached by waves generated from either an ice avalanche or ice calving event (Iribarren Anacona et al., 2015b), and at the Ventisquero Negro Glacier – dam breach due to increased outflow after a period of prolonged and intense rainfall (Worni et al., 2012). The Ventisquero Negro Glacier and Río Los Leones Valley events also represent the only moraine-dam failure sites for which detailed geomorphic studies have been conducted post-GLOF. Through combining field measurements with satellite-derived DEMs and a 2-D dynamic dam break model, Worni et al. (2012), for example, estimated a flood volume and peak discharge of 10×10^6 m^3 and 4100 m^3 s^{-1}, respectively, for the 2009 Ventisquero Negro GLOF event. For the Río Los Leones event, Harrison et al. (2006) conducted a detailed field-based sedimentology assessment of the post-GLOF floodplain, estimating a downstream debris deposit volume of ~2×10^6 m^3. Estimations of flood volumes and peaks discharges are also available for several other moraine dam failures in Patagonia (see Iribarren Anacona et al., 2014). One such event, occurring at Laguna del Cerro Largo in 1989, is possibly the largest moraine-dam failure outburst reported worldwide, with an estimated flood volume of 229×10^6 m^3 (Hauser, 2000; Clague and Evans, 2000). However, none of the GLOF events reported have been directly observed by river gauging instruments and consequently flood estimations are largely based on empirically-derived lake area-volume relationships that contain large uncertainties (e.g. ±71% - Iribarren Anacona et al., 2014).

In December 2015 a large GLOF event occurred at Lago Chileno in southern Patagonia causing extensive damage to a vegetated alluvial plain located immediately downstream of the breach before entering an ice-dammed lake located on the eastern flank of Exploradores Glacier and then draining into the Río Exploradores. Prior to the GLOF event, Lago Chileno was notable in that it had undergone a period of rapid expansion and, at the point of outburst, represented the third largest moraine-dammed lake to have failed in Patagonia. However, unlike other moraine-dammed lakes in Patagonia, Lago Chileno had previously regulated water levels because it had a well-established outflow channel, raising questions about the process of failure. This study presents a detailed analysis of the Chileno Valley comprising five main elements: (1) a quantification of the downstream geomorphological impacts of the GLOF event; (2) description of the sedimentology of the post-GLOF floodplain; (3) an assessment of the bathymetry of Lago Chileno; (4) an estimation of volume, discharge, velocity and duration of the outburst flood; and (5) an evaluation of possible triggering mechanisms and lake draining scenarios. These elements were assessed through the use of topographic and bathymetric surveys conducted during a field campaign in February 2017, satellite-derived imagery and Digital Elevation Models (DEMs) collected prior to and after the outburst and downstream flood hydrograph data. Given the sparsity of information regarding GLOF processes in Patagonia, this study represents a valuable contribution towards future GLOF hazard and risk appraisals in this region.

2. Study area

The Chileno Valley (46.52°S, 73.12°W) forms part of the Cordón Las Parvas, a partially glacierized mountain range located northeast of the Northern Patagonia Icefield (NPI) in Chile. Glaciers in this region exist in a humid and maritime climate and are nourished by westerly airflows that deliver large amounts of precipitation year-round (Carrasco et al., 2002), falling as snow above the 0 °C isotherm (2000 m elevation in summer and 900 m in winter (Matsuoka and Naruse, 1999; Barcaza et al., 2009)). The NPI, for example, receives an estimated average snowfall of 6.7 m a^{-1} (Escobar et al., 1992); however, precipitation totals are reduced on the eastern side of the Andean divide (Masiokas et al., 2008). Patagonian glaciers have generally experienced negative mass balance conditions since the end of the LIA in response to atmospheric warming (e.g., Villalba et al., 2005; Bown and Rivera, 2007) and changes in the amount and type of precipitation (e.g., Giese et al., 2002; Montecinos and Aceituno, 2003; Rasmussen et al., 2007) .

The Chileno Valley is headed at its eastern extent by the Chileno Glacier, which is fed by a single tributary descending from a steep-sided and heavily crevassed accumulation zone formed on the western flanks of three mountain peaks (maximum elevation of ~2100 m a.s.l.). Having reached a length of around 2 km at its presumed LIA maximum, Landsat 5 satellite imagery indicates that Chileno Glacier retreated (~470 m) and thinned considerably by 1987 leaving behind a large terminal moraine (~80 m in height) and exposing steep-sided lateral moraines on either side of the glacier trunk (~260 m in height in places). Notably, by 1987 three water bodies had also begun to form in pro- and supraglacial locations across terminal regions of the heavily debris-covered

trunk of Chileno Glacier. These water bodies later coalesced as the glacier continued to retreat between 1987 and 2002 (~23 m a^{-1}), forming a singular proglacial lake (Lake Chileno) with an area of 0.31 km^2. In response to an increased rate of glacial retreat (~70 m a^{-1}), Lake Chileno expanded rapidly during the following 13 yr and prior to the 2015 GLOF event had more than doubled its area to 0.75 km^2. Lake Chileno drains via an outflow channel cut through the LIA terminal moraine into what was a vegetated alluvial plain for 900 m before dissecting a LIA lateral moraine formed by Exploradores Glacier and then flowing into a large ice-dammed lake. Located on the eastern flank of Exploradores Glacier, this ice-dammed lake began to form in 2003 and has since expanded rapidly, covered an area of 1.15 km^2 in 2016. Water from the ice-dammed lake drains into the Exploradores River that terminates in the Cupquelán Fjord located 37 km northwest of the Exploradores Glacier snout.

3. Methods

3.1. Field data

Field data for this study included (1) aerial imagery, (2) lake bathymetry measurements, (3) floodplain sedimentology observations and (4) river water level and temperature measurements. Datasets (1), (2) and (3) were acquired during fieldwork in February 2017, whilst dataset (4) was obtained from a Water Level Sensor (WLS) installed in the Exploradores River by a team from the Catholic University of Chile on the 26 November 2015. The WLS system consisted of a Solinst Leveloger Edge (inserted into the water) and a Solinst Barologger Edge. The latter was set above the water level in order to record fluctuations in atmospheric pressure. Information obtained from these four data sources was supplemented by field photography taken during separate field expeditions in 2010 and 2014.

For detailed 2-D and 3-D topographic mapping of the post-GLOF terrain, aerial imagery of the Chileno Valley was collected using a fixed-wing UAV mounted with a downward facing 16.2 megapixel Sony NEX-5N digital camera. The fixed-wing UAV platform used was based on the Skywalker X8 airframe described by Ryan et al. (2015) and detailed in Table 1. Autonomous control of the UAV was made possible through the installation of a Pixhawk autopilot UAV module that combines an L1 frequency (1575.42 MHz) GPS, two inertial measurement units (IMUs), a compass, and a barometer. Image-acquisition was triggered automatically every three seconds by the mounted camera (equivalent to a horizontal displacement of ~50 m) providing a forward overlap of ~92%. Moreover, a 50% horizontal or side image overlap was achieved by using a 300 m flight line separation width. To optimise image quality, the camera was pre-set for a fixed exposure of 1/1000 s, an ISO of 100 and F-stop of 8. The Sony NEX-5N has a 16 mm fixed-focus lens (equivalent to 24 mm for a 35 mm film camera), which gives an FOV of 53.1 by 73.7° yielding a ground footprint of 900 × 600 m and an image resolution of <0.5 m when the pre-programmed cruising altitude of 600 m a.s.l. was reached.

Table 1
Specifications of the fixed-wing UAV and bathymetry boat.

Fixed-wing UAV specifications	
Airframe model	Skywalker X8 (www.hobbyking.com)
Construction material	Expanded Polypropylene (EPP)
Wing-span	2.12 m
Power-unit	Two 5 Ah (14.8 V) 4-cell lithium polymer batteries
Weight	~3 kg (including 0.7 kg camera)
Cruising speed	55–70 km per hour
Flying range	~60 km
Camera	Sony NEX-5 N
Cost	<2000 USD (including camera)
Bathymetry boat specifications	
Construction material	Expanded Polypropylene (EPP)
Dimensions (length × width)	910 mm × 590 mm
Power-unit	2 × 7 Ah (6 V) lead acid batteries
Weight	<5 kg
Control system	2.4 GHz radio control system
Cruising speed	6 km per hour
Battery life	90 min
Depth frequency	150 KHz
Depth range	~150 m
Cost	<500 USD

The bathymetry survey of Lake Chileno was conducted using a custom-built remote-controlled boat (see Table 1). The hull of the boat was milled from expanded polystyrene and was based on a simple low speed catamaran design. Once deployed, bathymetry measurements were acquired by the boat every three seconds using a 150 KHz thru-Hull Depth transducer connected to Actisense Dst-2 active depth sounder module. This sounder module was additionally fitted with a sonar control system, including an ATMega 328 microcontroller, an uBlox NEO-6 GPS unit and an RFM69HW radio transceiver that was used during debugging. The control system for the boat itself was a standard 2.4 GHz radio system that allowed only manual control. Propulsion was made possible through the installation of two brushed 12 V motors that were attached to two independent propellors via traditional prop-shafts mounted in each hull. Power was provided by a 7 Ah 12 V battery pack, allowing for around 90 min of operation between recharges. Steering was achieved using independent rudders driven by standard radio control servos mounted on each hull. The rudders were arranged to be directly in the flow of water from the propellers in order to improve steering responsiveness.

3.2. Aerial image orthorectification, DEM extraction and DEM differencing

The orthorectification and mosaicking of the aerial imagery acquired, as well as the extraction of 3-D data from overlapping image pairs, was performed using the Agisoft Photoscan Pro software package (http://www.agisoft.ru/products/photoscan). These processing procedures were realised by Photoscan through the implementation of a fully automated 2-stage workflow. The first stage involves image alignment using the structure-from-motion (SFM) digital photogrammetry technique. Best suited for imagery acquired at multiple viewpoints by a moving sensor, SFM calculates camera positions and the orientation of image scenes without the input of known 3-D positional data (Ullman, 1979; Westoby et al., 2012). Instead, these parameters are calculated through the identification of corresponding high contrast features within regions of image overlap. These image features are then used to obtain the relative position of each image within a sequence, to solve camera calibration parameters (e.g., focal length and distortion coefficients) and to produce a sparse 3-D point cloud (Ryan et al., 2015). Once aligned, the SFM image-space coordinates can be transformed to an absolute coordinate system using x, y, z Ground Control Points (GCPs) obtained from a reference map projection. In this case, 15 GCPs were manually selected from Sentinel-2 (x,y) and WorldDEM (z) satellite data (see Table 2) projected to the WGS1984 UTM (zone 18S) coordinate system. These two reference datasets were chosen due to their fair spatial resolution of 10 m (Sentinel-2) and 12 m (WorldDEM). The GCPs were selected in areas of good satellite image quality (e.g., cloud/shadow free and away from elevation errors) that were sparsely vegetated and judged to have undergone little or no geomorphic changes as a result of the GLOF (see Fig. 1). The eastern section of the Chileno Valley, in particular, was excluded from the GCP selection process due to a high concentration of WorldDEM elevation errors likely brought about by the steep terrain (Becek et al., 2016).

During the second stage of image processing, Photoscan applies a pixel-based multiview reconstruction algorithm to all aligned images in order to produce a 3-D polygon mesh. This mesh was then used for the extraction of a DEM and subsequently the generation of an orthorectified image mosaic for all overlapping portions of the image

Table 2
Satellite data used in this study.

Satellite data	Spatial resolution (m)	Acquisition date	Utility	Source
Satellite imagery				
Landsat 5	MS 30, PAN 30	09 February 1987	LV, GV	USGS
Landsat 7	MS 30, PAN 15	18 January 2002	LV, GV	USGS
WorldView-2	MS 1.85	24 February 2014	VA	ESRI
Landsat 8	MS 30, PAN 15	21 January 2015	LV, GV, VA	USGS
Landsat 8	MS 30, PAN 15	08 January 2016	LV, GV, VA	USGS
Landsat 8	MS 30, PAN 15	12 March 2016	LV, GV, VA	USGS
Sentinel-2	MS 10	05 February 2017	VA, GCPs	ESA
Elevation data				
WorldDEM	12	22 January 2011–28 August 2014 (32 acquisitions)	DD, GCPs	DLR/ADS

MS - Multispectral; PAN - Panchromatic; LV/GV - Lake/Glacier variations; VA - Visual analysis; GCPs - Ground control points; DD - DEM differencing; USGS - US Geological Survey; ESRI - Environmental Systems Research Institute; ESA - European Space Agency; DLR - German Aerospace Center; ADS - Airbus Defence and Space.

sequence. This process was applied using Photoscan's medium quality setting, resulting in a DEM and ortho-image resolution of 0.5 m. For the DEM differencing procedure, the UAV-derived DEM was first resampled to 12 m using a bilinear interpolation technique, matching the spatial resolution of the WorldDEM. A surface elevation change raster dataset was then created by subtracting the WorldDEM from the UAV-derived DEM.

3.3. Satellite data

Capturing the three-dimensional terrain of the Chileno Valley prior to the GLOF event, the WorldDEM was the primary satellite dataset used in this study. The WorldDEM is a high precision standardised global DEM generated through the merger of TanDEM-X Synthetic Aperture Radar (SAR) data acquired between 2010 and 2014. This elevation dataset was chosen over other freely available DEMs that offer near-global coverage (e.g., the Shuttle Radar Topography Mission (SRTM) and ASTER GDEM datasets) due to (1) the temporal proximity of its acquisition to the GLOF event, (2) its improved spatial resolution (12 m), and (3) its superior absolute and relative vertical accuracies of <4 m (Riegler et al., 2015). Elevation data for our specific study area was contained within the S47W074 WorldDEM tile that has been generated from 32 individual TanDEM-X passes with acquisition dates ranging from 22 January 2011 to 28 August 2014. As secondary satellite data sources, five Landsat satellite images acquired between 1987 and 2017 were used for the purposes of monitoring glacier, glacial lake and geomorphology changes in the Chileno Valley (Table 2). These were further supplemented by WorldView-2 and Sentinel-2 satellite image acquired in February 2014 and 2017, respectively.

3.4. Flood estimations

The peak discharge (Q) and flow velocity (V) of the outburst flood were estimated indirectly along two cross sections located close to the flood breaching point (Fig. 6). Spanning the maximum extent of the flood, these two cross sections were selected along reaches where (1) the upper limit of the flood could be clearly identified (through water marks and areas of stripped soil), (2) the flow was likely to be unidirectional, and (3) post-GLOF changes in channel geometry were limited compared to other flood affected zones. The high levels of channel erosion and sediment deposition present elsewhere along the floodplain prevented the analysis of further flood cross sections. Using geometric information obtained from the UAV DEM, V was estimated using the Manning equation, assuming a uniform flow, whilst Q was estimated using the slope-area method (for specific formulas see Kershaw et al. (2005)). Both methods represent standard methods for reconstructing floods in ungauged rivers (e.g., Webb and Jarrett, 2002) and have been used previously to estimate the hydrological parameters of GLOFs (e.g., Kershaw et al., 2005). With reference to values presented by Arcement and Schneider (1989), roughness coefficients (a key parameter of the Manning equation) were manually estimated using pre-GLOF field photography (acquired in 2010 and 2013) and WorldView-2 satellite imagery (Table 2). Additionally, an average slope parameter was extracted from the UAV DEM using a 130 m central transect running parallel to the river flow and intersecting both cross sections. Logged at 10 min intervals, the direct measurements collected by the WLS were converted into river Q with the use of a stage-discharge curve calibrated with Q and V data surveyed in the field with a Sonteck Acoustic Doppler Current Profiler (ADCP). Field data was collected on four separate dates with Q ranging from 27 to 186 $m^3\ s^{-1}$.

3.5. Uncertainty analysis

In this study there are two main sources of uncertainty: (1) the geomorphic change analysis derived from DEM differencing; and (2) the flood estimations derived from a discharge rating curve and the Manning equation. In order to address the first of these sources, the vertical accuracy of the UAV-DEM was assessed relative to the WorldDEM reference dataset. To estimate this relative accuracy (*RA*), vertical errors calculated during the Photoscan co-registration process were combined through simple error propagation theory (Taylor, 1982), with those calculated for manually sampled control points:

$$RA = \sqrt{A^2 + B^2}$$

where A^2 is the Root Mean Square Error (RMSE) of elevation differences ($RMSE_z$) for the 15 co-registration GCPs and B^2 is the RMSE of elevation differences for 1280 control points sampled in stable areas unaffected by the GLOF. Prior to calculation of B^2, elevation difference values exceeding ±2 standard deviations were treated as outliers and removed (reducing the control point sample to 1213). The resulting relative vertical accuracy equated to ±1.5 m and this error is therefore attributed to all elevation change measurements reported. However, further elevation uncertainties may have been introduced by the inclusion of vegetation within the WordDEM elevation dataset. The influence of these uncertainties is likely to be limited for the Chileno Valley floodplain as, pre-GLOF, the majority of the area was covered by a low layer of shrubs (~50 cm in height). However, uncertainties may be more pronounced in the far eastern portion of the alluvial plain where areas of woodland (~2–5 m in height) existed prior to the GLOF, adjacent to the LIA moraine. The accuracy of the DEM differencing procedure is also influenced by the horizontal errors introduced by (1) the co-registration process and (2) the absolute horizontal accuracy of the WorldDEM and Sentinel-2 reference data. The first of these factors was calculated during the co-registration process and equated to 4 m, less than half of the pixel resolution of the reference datasets. The second factor was not calculated for the Chileno Valley specifically, however, global estimates suggest values of <6 m and 12.5 m for the

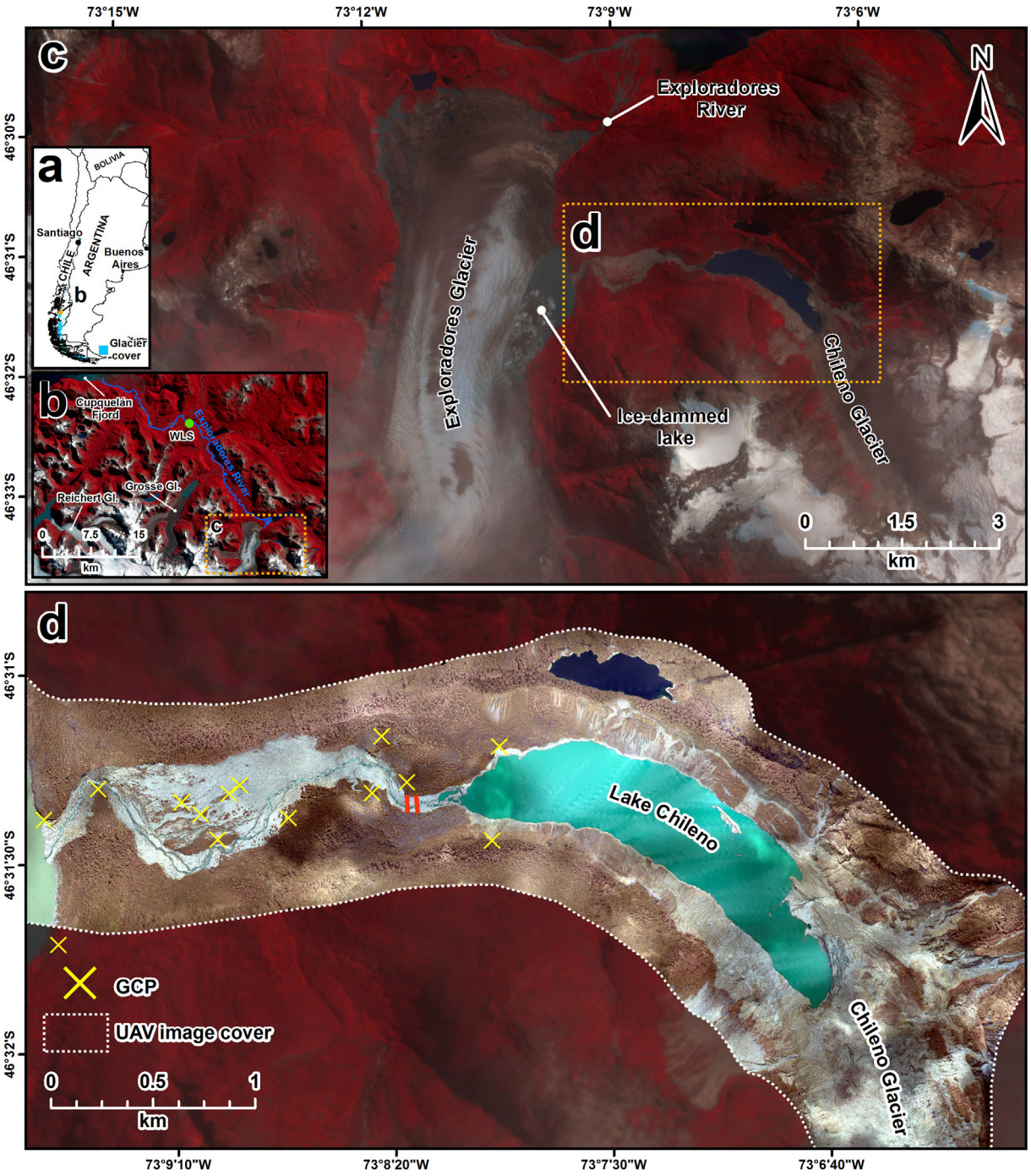

Fig. 1. Location of the study site within Patagonia (a), in its regional context (b) and in relationship to Exploradores Glacier (c). Detail of the Chileno Valley is shown in panel (d). The location of the Water Level Sensor (WLS) installed in the Exploradores River is marked in panel (b), whilst the 15 Ground Control Points (GCPs) used for the processing of the aerial imagery are marked in panel (d).

WorldDEM and Sentinel-2 datasets, respectively (Drusch et al., 2012; Riegler et al., 2015).

The uncertainties associated with the flood estimations presented are difficult to quantify. In regards to the Q values derived from the WLS data, uncertainties relate to the use of a stage-discharge relationship generated at low to moderate flows to estimate Q during a high-magnitude GLOF event. In this case, for example, the estimated peak Q of the GLOF event was more than two magnitudes higher than that measured in the field. In regards to the in-direct estimations of Q and V, uncertainties relate to the simplicity of the technique applied, the difficulties determining and applying Manning's roughness coefficients for GLOF events and the accurate representation of channel geometry for each cross-section. This issue is discussed further in Section 4.1.

4. Results and discussion

4.1. Flood volume, discharge and velocity

Visual analysis of MODIS satellite images constrain the initiation date of the GLOF to between the 4 December 2015 and 7 January 2016. WLS sensor data for this period revealed that Q for the Rio Exploradores experienced three distinct peaks between 9 and 23 December (herein referred to as peaks 1, 2 and 3) before increasing

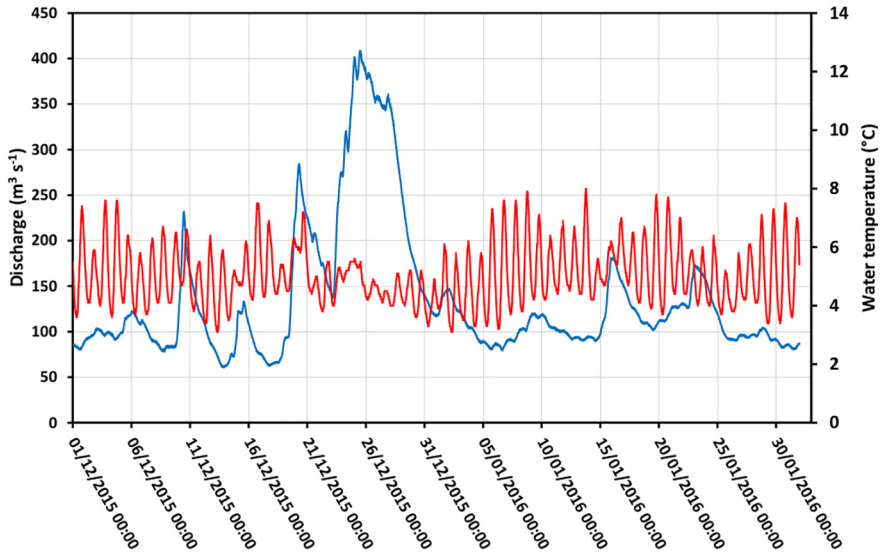

Fig. 2. River discharge (blue) and air temperature (red) measured between 1 December 2015 and 1 February 2016 by a WLS installed on the Exploradores River (see Fig. 1 for location).

rapidly to a fourth peak of 408 $m^3 s^{-1}$ measured at 13:30 on 25 December (peak 4 - Fig. 2), a value more than three times the magnitude of the Q average during low-flow conditions recorded between December 2015 and January 2016. We assume that the fourth peak represents the peak Q for the GLOF event, which occurred ~26 km upstream at Lake Chileno.

Calculating the volume of the GLOF using the flood hydrograph is complicated by uncertainties related to the precise timing of the GLOF event. Once the GLOF was triggered, flood water from Lago Chileno was likely influenced by a number of factors prior to reaching the WLS site, such as: (1) the interface with an ice dammed lake; (2) passage through sub-, en-, and supra-glacial channels of the Exploradores Glacier ice dam; (3) possible interface with Lake Bayo - which may represent a partial drainage point; (4) passage ~21 km downstream of the Exploradores Glacier outlet – a stretch of Rio Exploradores that receives additional water from a number of other glacierised and non-glacierised basins, some of which include glacial lakes. Each of these factors have the ability to enhance, lessen and/or delay flood waters, in doing so, alter the flood hydrograph. For example, due to the almost immediate interchange between their falling and rising limbs, it is possible that peaks 3 and 4 represent a single directly-linked flood event. In this scenario, the two Q peaks could then represent either (1) a dual release of GLOF water from Lake Chileno or (2) the existence of a second outburst event from the ice-dammed lake, possibly triggered by the input and impact of the Lake Chileno GLOF. Here, both of these scenarios are discounted primarily on account of evidence provided by the WLS water temperature measurements. Between December 2015 and January 2016, for example, a distinct diurnal variation in water temperatures is evident, a characteristic typical of other glacierised river catchments around the world (Brown et al., 2006). However, upon the initiation of the fourth flood event on 23 December 2015, these diurnal variations dampen considerably, with average water temperatures recorded throughout the duration of this event decreasing to 4.6 °C, 0.4 °C lower than the average of previous measurements made in December (Fig. 2). These changes in water temperature are assumed to be the result of (1) the large Q and V of the flood waters (reducing the time available for heat transfer) and (2) the input of a significant volume of relatively cold water from Lake Chileno - the water temperature of other GLOFs in Patagonia have been reported to be as low as 4 °C (e.g., Dussaillant et al., 2010). Assuming that peak 4 represents the Lake Chileno outburst, the flood continued for 7 days, 19 h, and 20 min during which time an estimated 105.6 $\times 10^6$ m^3 of water flowed past the WLS site.

The indirect measurements of GLOF Q and V close to the location of the initial breach are shown in Fig. 3. Due to the close proximity of cross sections 1 and 2, estimations of bankfull Q and V are similar, ranging between 5307 and 5746 $m^3 s^{-1}$ and 7.76–7.84 m s^{-1}, respectively. The accuracy of these estimations is difficult to assess primarily due to uncertainties related to the use of Manning's roughness coefficients. For example, in this case, we only accounted for flood energy losses in relation to cross-channel grain roughness. However, in reality, further energy losses would have occurred due to turbulence, sediment transport and channel expansion through erosion. This underestimation of total energy losses means that Q estimations using Manning's roughness coefficients are often overestimated (Cenderelli and Wohl, 2001; Lumbroso and Gaume, 2012). Furthermore, additional uncertainties arise related to the limitations of manual determination of roughness coefficients from photography and satellite imagery and the use of a static roughness value. In regards to the latter point, the river channel at cross sections 1 and 2 both widened and deepened during the GLOF event, altering the cross-channel grain roughness. As a consequence of the uncertainties discussed above, the indirect measurements of Q and V are seen as first order approximations.

Despite the uncertainties discussed, the magnitudes of the direct and indirect GLOF measurements are not unprecedented in Patagonia. The Cerro Largo GLOF in March 1989 released an estimated 229 $\times 10^6$ m^3 of water and is regarded the largest moraine-dammed lake outburst recorded worldwide in historic time (Clague and Evans, 2000; Iribarren Anacona et al., 2015a). In comparison, a moraine dam failure at Lake Engaño in March 1977 released an estimated 12–13 $\times 10^6$ m^3 of water with discharges surpassing 10,000 $m^3 s^{-1}$ (Iribarren Anacona et al., 2015b). More recently in May 2009, the moraine dammed lake at Ventisquero Negro Glacier failed releasing an estimated 10 $\times 10^6$ m^3 of water and generating peak discharges of 4100 $m^3 s^{-1}$ (Worni et al., 2012). Incidentally, none of the moraine-dammed lake failures recorded in Patagonia have been measured directly. The two features that mark the Lake Chileno GLOF out as unusual on a Patagonian perspective are (1) the long duration of the flood and (2) the volume of the flood in comparison to lake drainage evidence. The Ventisquero Negro and Lake Engaño GLOFs, for example, have been estimated to have lasted for between 3 and 10 h (Worni et al., 2012; Iribarren Anacona et al., 2015b). Similar short GLOF durations have been reported elsewhere in the world (e.g., British Columbia - Clague and Evans, 2000). In terms of drainage volume, field observations of water marks at Lake Chileno suggest that the lake level dropped by ~2 m. Using this measurement

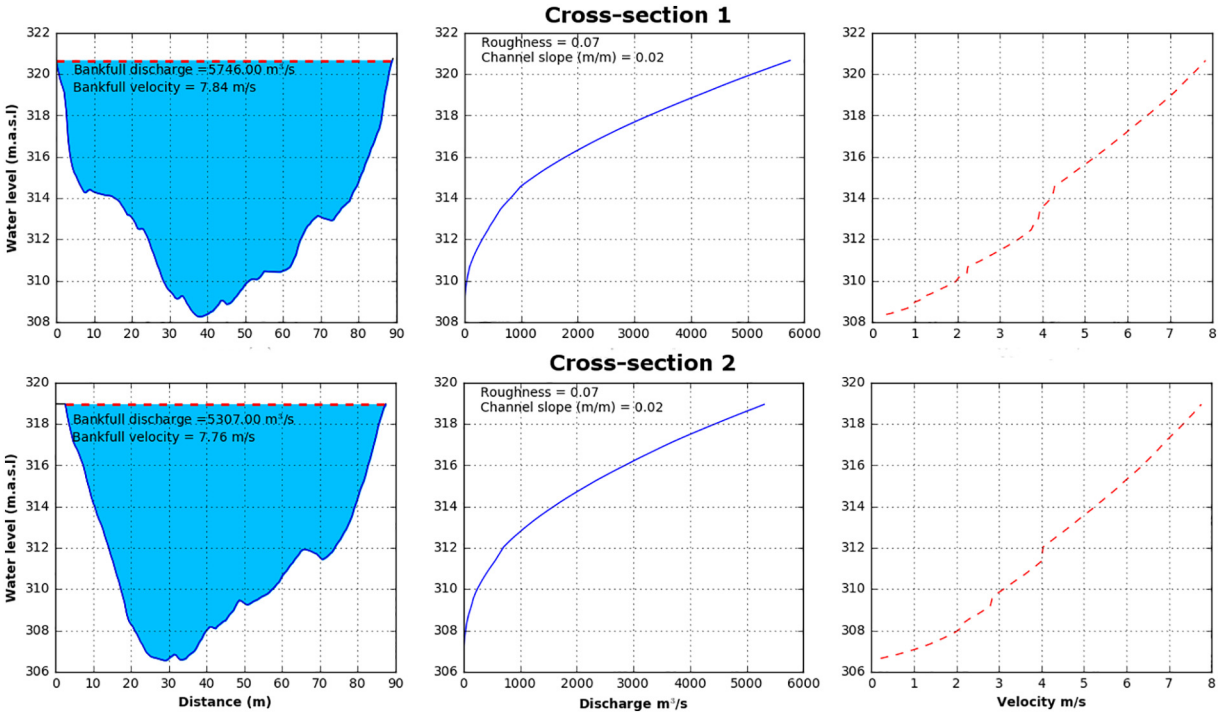

Fig. 3. Indirect measurements of GLOF discharge and velocity for two channel cross sections located in the Chileno Valley (see Fig. 6).

and a lake outline delineated from Landsat 8 imagery acquired in January 2015, the lake was estimated to have drained only ~1.85 $\times 10^6$ m^3 of water. These two factors therefore support a hypothesis that the flood was a multi-stage event, with waters being released over a prolonged period, and that the flood was likely augmented by precipitation inputs and water from the ice dammed lake. The drainage of the Lake Chileno was also likely increased through the input of significant amounts of debris and water during a large debris-flow event, which may have triggered the initial moraine breach (see Sections 4.3 and 4.4).

4.2. Geomorphic impacts and floodplain sedimentology

The downstream geomorphic impacts of GLOFs in Patagonia have been studied in only a few cases (e.g. Hauser, 2000; Harrison et al., 2006; Worni et al., 2012), a situation brought about due to the sporadic nature of their occurrence, their often remote location and the necessity of terrain information collected prior to and after the flood events. Here, the availability of relatively high-resolution DEMs derived from satellite data (WorldDEM – acquired in 2011/14) and a UAV field survey (acquired in February 2017) enabled a

Table 3
Observed sedimentology of seven sites located in the Chileno Valley. Corresponding imagery and their acquisition location are shown in Fig. 7 and Fig. 5, respectively.

Unit	Location	Clast data	Diamict code and associated data	Interpretation
1. Exposed in situ deposits (Fig. 7a)	Proximal zone. Incised by present river and forms lowest sedimentary unit.	SR-SA. Up to 1 m b-axis. Blocky	Dmm and Dms. Unit up to 4 m thick. Massive silt and sand matrix.	In situ subglacial till that has been incised by flood.
2. Resedimented unit (Fig. 7b)	Proximal zone. 6 m above present channel.	No clasts	Dms(r). Rhythmites of fine sand and silt.	Lake deposits moved by GLOF ave.
3. Boulder lobes and splays (Fig. 7c & d)	Transitional zone. Close to present channel and on distal sides of GLOF apron.	Large clasts form braking blocks; others have moved on sub-clast cobble train. Clasts SR-SA, blocky and b-axis up to 6 m. Many imbricated.	Gch. Sma ll perched clasts on top of large boulders.	High energy flow moving large cobbles; some debris flow activity and rapid dewatering.
4. Isolated boulders (Fig. 7e)	Transitional zone. Within present channel.	Mega clasts up to 7 m b-axis. Blocky and SR. Strongly imbricated.	Mega clasts	Some clearly entrained during GLOF, others in situ.
5. Clasts in fine sand silt matrix (Fig. 7f)	Proximal and transition zone.	Large clasts up to 4 m b-axis. SR. Inverse grading shown.	Dms(r). Form small lozenge-shaped deposits, erosional remnants of larger unit. Matrix-supported in places.	May represent a pre-existing debris flow unit that has been incised, or isolated debris flows associated with hyper-concentrated flows.
6. Gravel splays (Fig. 7g)	Distal zone.	Units comprising large clasts up to 1.5 m b-axis, SR-SA. Form boulder runs. Units of small clasts form within-channel gravel splays; fine gravel matrix. Clasts up to 20 cm b-axis.	Clasts with little matrix. Imbricated.	Fluvial deposits. Form boulder berms.
7. Sand units (Fig. 7h)	Far distal zone.	Isolated clasts and clast runs.	sG. Found as sand/gravel sheets and also in lee of large boulders.	Associated with water floods during waning of GLOF flow.

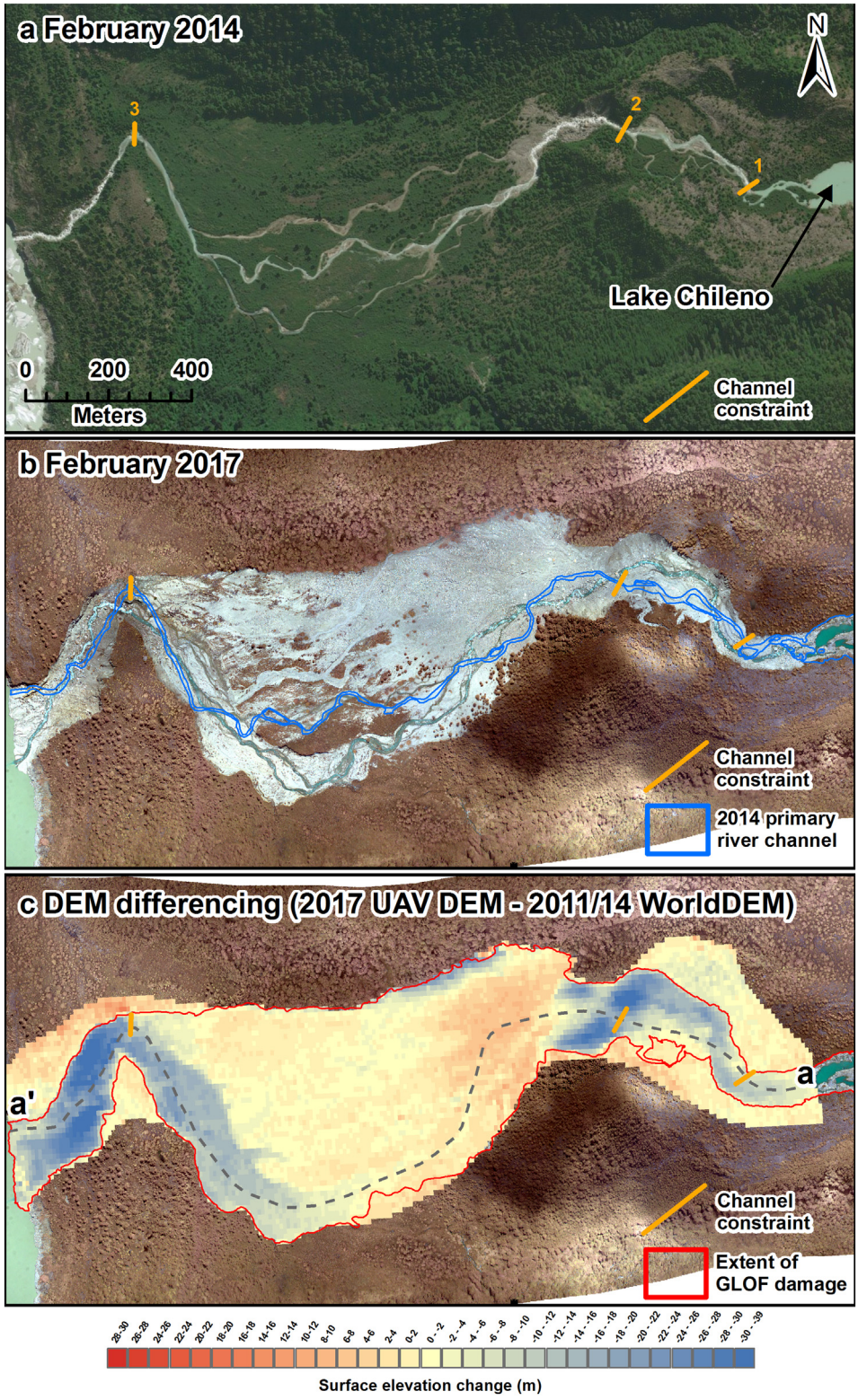

Fig. 4. Geomorphology of the Chileno Valley before (a) and after (b) the GLOF event that occurred in December 2015. Post-GLOF surface elevation changes are shown in image (c).

detailed analysis and quantification of valley erosion and deposition generated by the Lake Chileno GLOF. For simplicity the description of these impacts is sub-divided into three reaches of the Chileno Valley: (1) the proximal channel; (2) the alluvial plain; and (3) the distal channel (see Fig. 6) Field observations describing the sedimentology of seven sites located in the proximal channel and alluvial plain is presented in Table 3.

The impacts of the Lake Chileno GLOF on the valley below are visually illustrated in Figs. 4–7. Impounded by the ridge of the overdeepened deglaciated basin of Chileno Glacier, Lake Chileno was initially drained via an overflow outlet located ~550 m upstream of an incised LIA moraine. Pre-GLOF, this overflow channel met two constraining points along the proximal channel (see Fig. 4a), where it dropped in elevation by ~6 m and ~48 m along reaches of 50 m and 230 m, respectively.

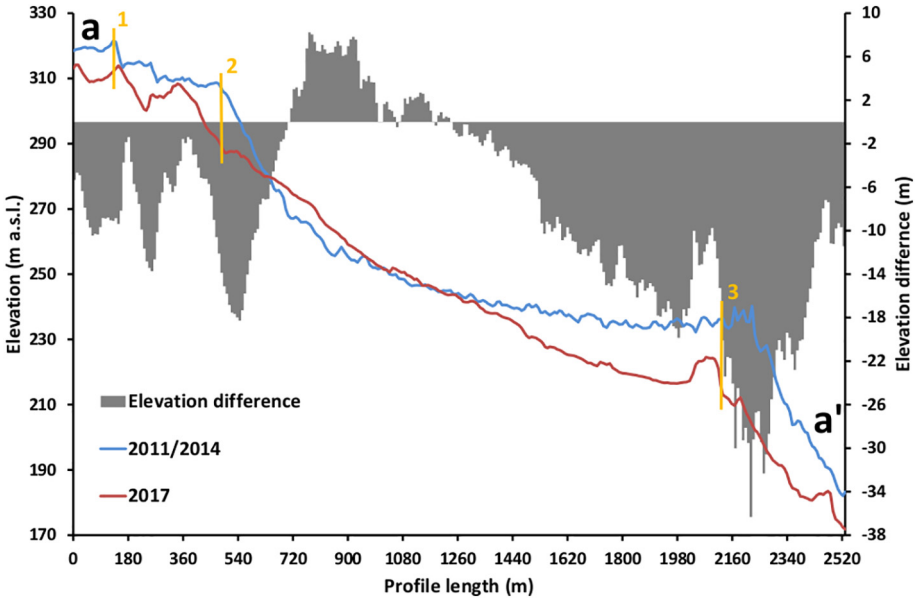

Fig. 5. Surface elevation changes along a longitudinal cross profile of the Chileno Valley (a-a' – see Fig. 4c).

Both of the channel constraints marked intersection points that are believed to be terminal moraines, features that were heavily eroded during the GLOF event. Located ~150 m from the lake outlet, the first of these channel constraints likely represents the initial breaching zone and is discussed as part of a multi-phase lake drainage scenario in Section 4.3.

Post-GLOF, the image and DEM comparisons presented depict a significantly modified river channel and valley bottom, characterised by areas of substantial valley/river bed erosion, sediment deposition (see Figs. 5 and 6) and river channel widening (Fig. 4). For the proximal channel, the river bed along the corresponding portions of the a-a' cross section, for example, lowered by an average of 8 ± 1.5 m. More prominently, however, flood inundation along this reach has resulted in considerable erosion of the channel margins leaving behind a generalised bowl-shaped morphology flanked on either side by steep-sided scarps (see Fig. 4b). At the initial breaching zone (channel constraint 1 – see Fig. 4a) the surface of the river channel lowered by an average of 8.9 ± 1.5 m with the river bank at this point widening by around 60 m. Furthermore, as a result of the GLOF, the river channel changed course and is now located 20 m to the south of the initial breaching zone (see Fig. 4b). Approaching what was the second channel constraint, the post-GLOF channel has in many sections widened by >100 m, these areas having lowered in elevation by >30 ± 1.5 m in places (Fig. 4c). The observation of areas of re-sedimented deposits along this reach also suggests that sediment was removed from Lake Chileno during the GLOF event (see Table 3 and Fig. 7b). The LIA terminal moraine that encompasses the proximal channel is at its peak around 35 m high. Post-GLOF erosion adjacent to its crest of this moraine (See Figs. 6 and 8), shows that it is composed of a series of stacked

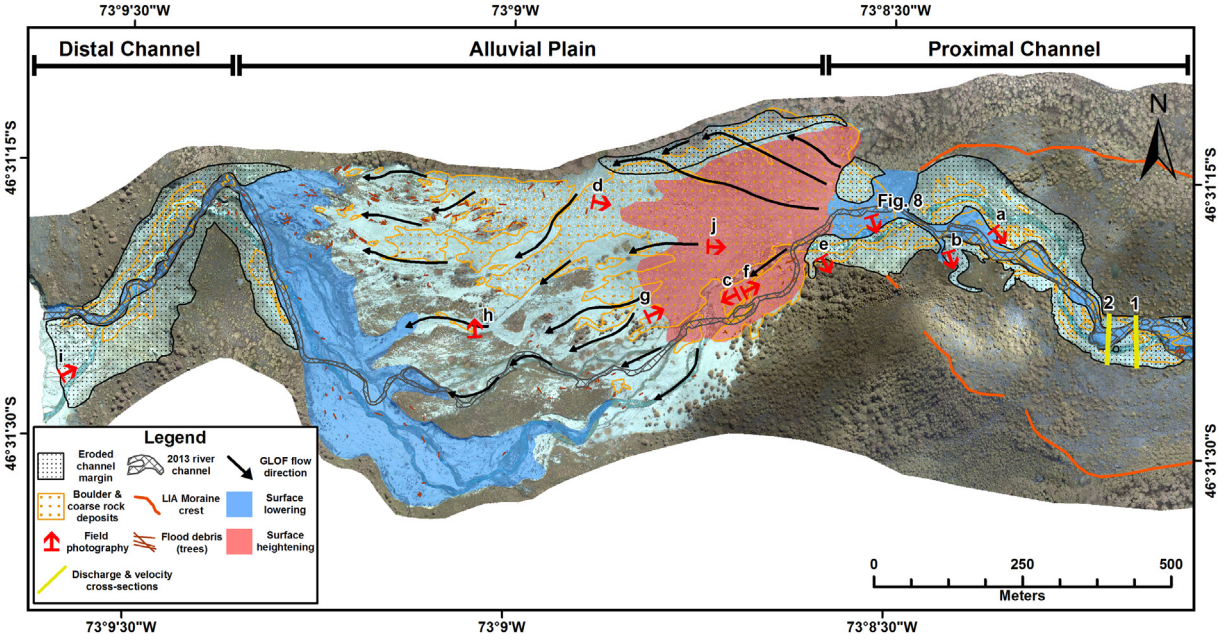

Fig. 6. Map of the Chileno Valley post-GLOF. Areas of significant channel erosion and surface deposition are delineated. Black arrows mark GLOF flow paths indicated by the presence of surface channels. Locations of the two flood discharge and velocity cross sections are also indicated.

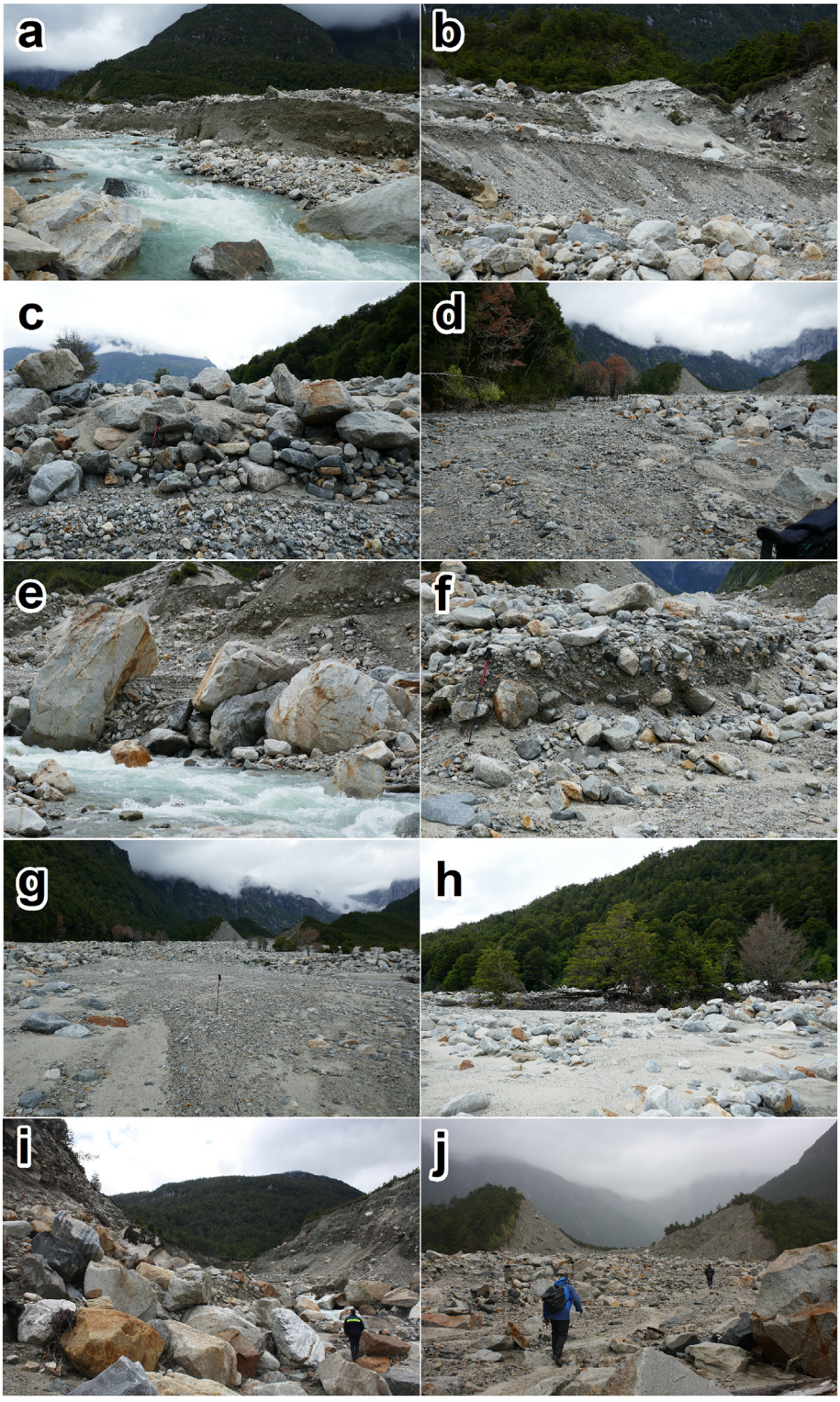

Fig. 7. Photographs taken during a field campaign in February 2017. Images illustrate the geomorphic impacts of the GLOF and the sedimentology of the floodplain. See Table 3 for details.

sedimentary units made of matrix-supported and poorly-sorted bouldery diamict. The units are from 1 to 2 m in thickness and dip downvalley at angles of up to 10°. Clasts are mainly subrounded to sub-angular and blocky, and up to 2 m in b-axis. The moraine is similar geomorphologically and sedimentologically to other LIA moraines in the valleys draining the NPI (e.g., Glasser et al., 2009) and record recession of the Chileno Glacier from the end of the nineteenth century (e.g., Harrison et al., 2007).

Downstream of the proximal channel, the valley bottom abruptly widens out into an open relatively low gradient (~5°) alluvial plain. Here, it is hypothesised that the bulk of the flood waters were initially directed towards the northern flank of the plain, eroding a roughly 40 m by 400 m section of dense forest before travelling eastwards as a broader sheet flow towards the distal channel. This process is evidenced by a large number of toppled trees which have been transported to the north eastern corner of the plain (see Fig. 6). As the flood energy was

Fig. 8. Field photography captured in February 2017 illustrating the post-GLOF erosion of the LIA moraine crest (see Fig. 6 for location). The crest of the LIA moraine is up to 35 m high and composed of a series of stacked sedimentary units made of matrix-supported and poorly-sorted bouldery diamict. The units are from 1 to 2 m in thickness and dip downvalley at angles of up to 10°. Clasts are mainly subrounded to sub-angular and blocky, and up to 2 m in b-axis.

reduced and flow diverged upon exiting the proximal channel, significant amounts of entrained sediment was deposited at the head of the alluvial plain, forming a ~340 m wide fan (see Figs. 4c and 7c,j). In this deposition zone (highlighted in red in Fig. 6), the post-GLOF surface rose by an average of 4.6 ± 1.5 m. Elsewhere on the alluvial plain, large areas of previously vegetated terrain have been stripped bare by the flood waters and replaced, along central flow paths, by boulders and coarse rock deposits (see Fig. 6). As discharge began to decrease, it is likely that the newly formed deposition zone acted as a barrier towards further flow along the northern reaches of the plain, instead forcing flow southwards, and in doing so, re-activating a previously inactive river channel running along the southern flanks of the alluvial plain. However, discharge at this later stage of the flood was still sufficient enough to result in considerable channel bed and marginal erosion along the southern channel, revealing incised banks of loosely consolidated sediment (made up of alluvial deposits and glacial till) in some places >15 ± 1.5 m in depth (see Fig. 6). The GLOF deposits within the southern channel were generally characterised by finer material (e.g., sand and gravel), indicative of slower flow conditions.

Prior to the GLOF, the main river channel of the Chileno Valley drained the alluvial plain via a relatively steep (~5°) and narrow ravine that fed directly into the ice-dammed lake located on the eastern margins of Exploradores Glacier. The impact of the GLOF along this reach was similar to that of the proximal channel, with the force of the flood waters resulting in significant basal and marginal erosion. Consequently, the post-GLOF channel along this reach has widened in some places by >130 m, with the surface elevation of terrain located either side of the former ravine lowering by a maximum of 38.8 ± 1.5 m. Having incised the LIA lateral moraine formed by Exploradores Glacier, the steep-sided scarps left behind by the GLOF along the distal channel revealed a large number of entrained boulders, many of which (as large as 8 m in width) have been deposited, together with material acquired farther upstream, along the channel bed (Fig. 7i). These deposits of larger material, both in the proximal and distal channel, have likely

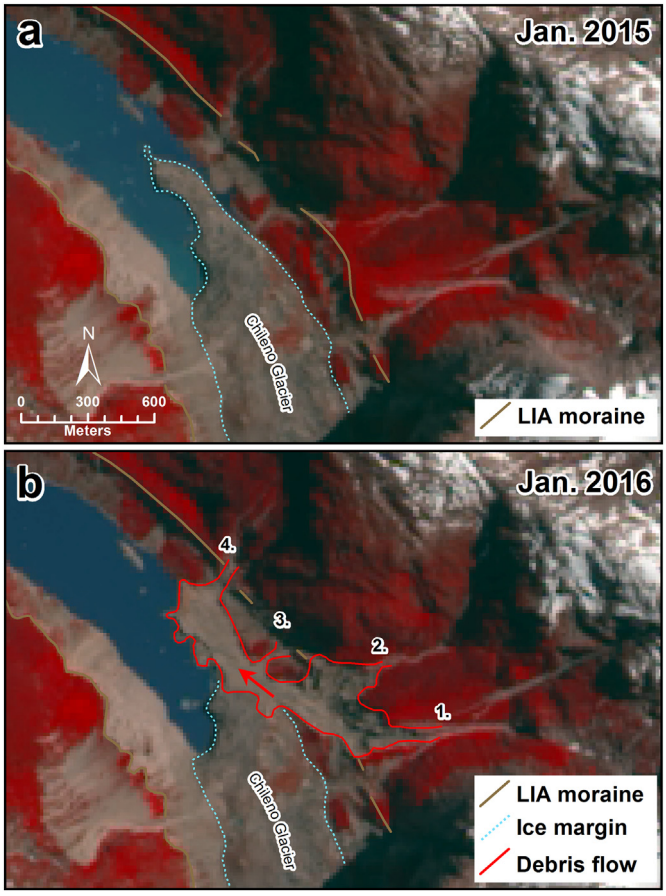

Fig. 9. Evidence of a large debris flow acquired from Landsat 8 imagery captured in 2015 (a) and 2016 (b). The primary (1) and secondary (2) pathways of the debris flow are marked on image (b). Additionally, two pre-existing gullies (3 and 4) also show evidence of widening post-GLOF and may have contributed further material to the debris flow.

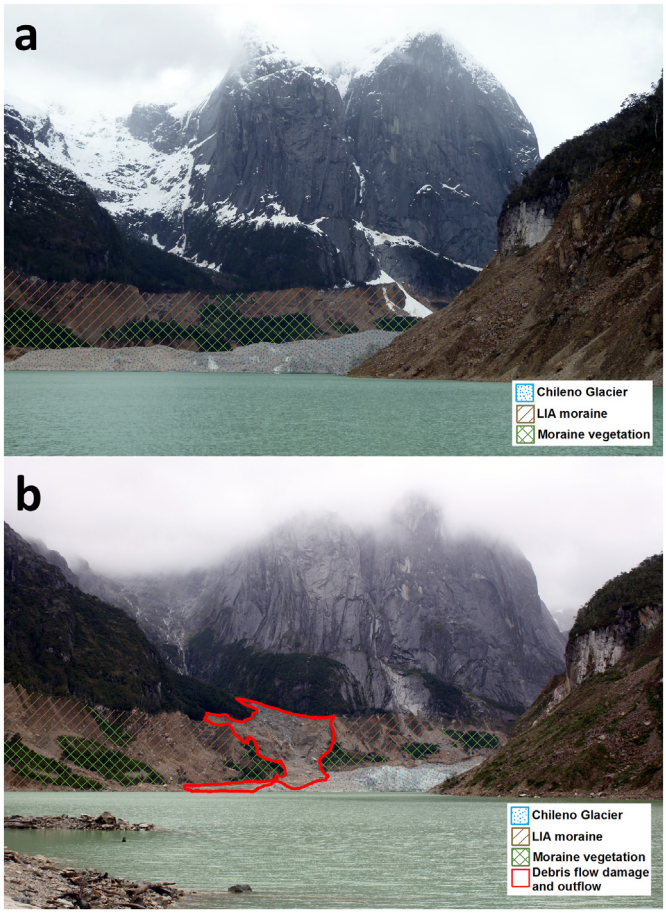

Fig. 10. Field photography captured in September 2010 (a) and February 2017 (b) illustrating the geomorphic impact of a potential debris flow.

been added to through structural failure of the steep-sided banks post-flood.

By combining surface elevation changes on pixel-by-pixel basis, the DEM differencing procedure enabled the quantification of the volume of sediment eroded and deposited downstream of the former limits of Lake Chileno (see Fig. 4c for extent). In total, it was estimated that 3,542,525 m^3 of material was eroded from flood affected areas (±16%), whilst 586,786 m^3 of material was deposited (±57%). Subsequently, it is estimated that a sediment load of at least 2,955,739 m^3 was transported into the adjacent ice-dammed lake in addition to material transported out of Lake Chileno during the GLOF event. The magnitude of the sediment erosion and deposition reported here is not unprecedented for GLOFs, although detailed observations of these processes are sparse due to the surveying difficulties discussed earlier in this section. In Patagonia, for example, GLOF deposits of 15 m in thickness have been observed, including boulders of 18 m in diameter, demonstrating the transport capacity of the flood waters (Harrison et al., 2006; Worni et al., 2012). Elsewhere, Vuichard and Zimmermann (1987) used field photography to estimate that ~3,000,000 m^3 of sediment was eroded and deposited during the 1985 Dig Tsho GLOF in the Khumbu area of Nepal. Furthermore, Osti and Egashira (2009) used field-based sediment depth samples to estimate that the 1998 Tam Pokhari GLOF in the Mount Everest region of Nepal deposited ~440,000 m^3 of material ~14 km downstream of its source.

4.3. GLOF trigger mechanism and lake drainage scenarios

GLOF events are often generated in response to a cascade of interlinking long-term and short-term processes (Haeberli et al., 2010; Worni et al., 2012). The Chileno Valley GLOF was pre-conditioned primarily by the climate-induced recession of Chileno Glacier since the end of the LIA. This process of glacial recession has, in turn, led to the development and subsequent rapid expansion of Lake Chileno from ~1987 onwards, a process that gradually increased the volume of lake water available for flooding. Downwasting of the Chileno Glacier has also resulted in the lateral debutressing of valley slopes and moraines located either side of the former ice limits. Augmenting trigger factors related to localised climatic change, hydrology, topography, geology and seismic activity, the stress release associated with this debuttressing may have increased slope instabilities (as has been documented for other glaciated regions (e.g., Augustinus, 1995; Holm et al., 2004; Cossart et al., 2008)) and the probability of mass movements entering Lake Chileno. Indeed, field and satellite observations of the upper Chileno Valley revealed a number of minor slope failures running along the steep flanks of the lateral morianes surrounding Lake Chileno, as well as a large incipient landslide developing on the north-facing valley side that overhangs the 2016 glacier terminus and encompasses an area of ~0.56 km^2. However, these features are unlikely to have transported enough material into Lake Chileno sufficient to initiate a GLOF. Instead, it is hypothesised that the 2015 GLOF event was initiated by a large debris flow event, which was subsequently identified in corresponding field and satellite imagery acquired prior to and after the flood (Figs. 9 and 10).

Originating primarily from two steep and largely non-vegetated mountain gullies located northeast of the Chileno Glacier terminus, this debris flow event resulted in the removal of a large portion of the lateral moraine running along the northern margins of the 2015 Chileno Glacier terminus, the contents of which formed a debris outwash plain that inundated northern sections of the glacier snout and partially infilled the adjacent areas of Lake Chileno (Fig. 9). With no large water bodies present at the head of these two gullies and snow cover likely to be minimal, it is assumed that this debris flow was triggered by an intense and/or prolonged rainfall event. Two pre-existing gullies, cutting into the northern lateral moraine adjacent to the 2015 glacier terminus, are also shown to have widened post-GLOF and may represent further evidence of such an event (see Fig. 9). Unfortunately, precipitation data from a localised meteorological station were not available to analyse this assumption further. However, large rainfall

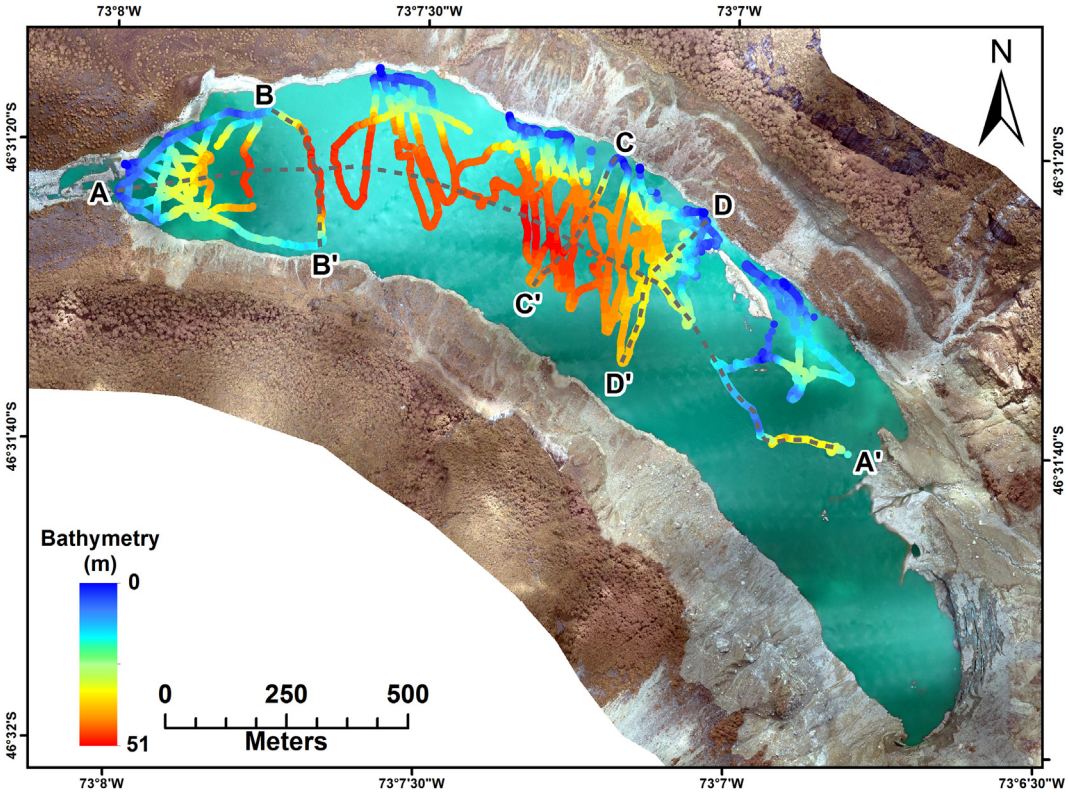

Fig. 11. Bathymetry survey of Lake Chileno, including the location of the four cross profiles shown in Fig. 12.

events are not uncommon in Patagonia. Worni et al. (2012), for example, stated that the 2009 Ventisquero Negro GLOF was partly triggered by sustained (180 mm of rain in a six-day period) and intense (50 mm of rain in the 48 h preceding the outburst) rainfall which led to increased outflow erosion and subsequent dam failure. More recently, a debris flow that inundated the town of Villa Santa Lucia (Northern Patagonia, Chile) on 16 December 2017, killing 12 people, was preceded by more than 114 mm of rainfall over a 24-h period (Iturrieta, 2017).

Once begun, it is proposed that the debris flow event initiated multiphase drainage scenario that culminated in the GLOF. Unlike other GLOF events triggered by mass movements documented in Patagonia (see Iribarren Anacona et al., 2015a) and other parts of the world (see Richardson and Reynolds, 2000), we do not believe that a large displacement wave, produced by the debris flow into Lake Chileno, played a significant role in the initiation of the flood. This conclusion is based on the fact that (1) field observations revealed no evidence of wave impact along the far western margins of Lake Chileno (only water marks left on rocks indicating the previous lake level) and (2) the snout of Chileno Glacier is likely to have borne the brunt of the initial impact of the debris flow (see Fig. 9b). Instead, we argue that the influx of sediment and water from the debris flow led to a progressive increase in the lake water level. This change in lake level would have increased the discharge of the overflow outlet that drains Lake Chileno, initiating gradual or sudden failure of the moraine dam (at channel constraint 1, Fig. 4a) through basal and marginal erosion. Energized by (1) the steep declining gradient of the pre-GLOF proximal river channel (see Fig. 5) and (2) the entrainment of sediment (as a result of the debris-flow and basal/marginal channel erosion), the flood waters would have then possessed the force required to cause the downstream geomorphic impacts described in Section 4.2.

4.4. Lago Chileno bathymetry

The results from the bathymetric survey of Lake Chileno are shown in Figs. 11 and 12. In essence they show that the lake is up to 50 m deep along its central axis and that the bottom of the lake is generally flat. Few bathymetric data from other Patagonian lakes are available to put these results in context (Loriaux and Casassa, 2013) but the available data from NPI glacial lakes suggest that Lake Chileno is shallower

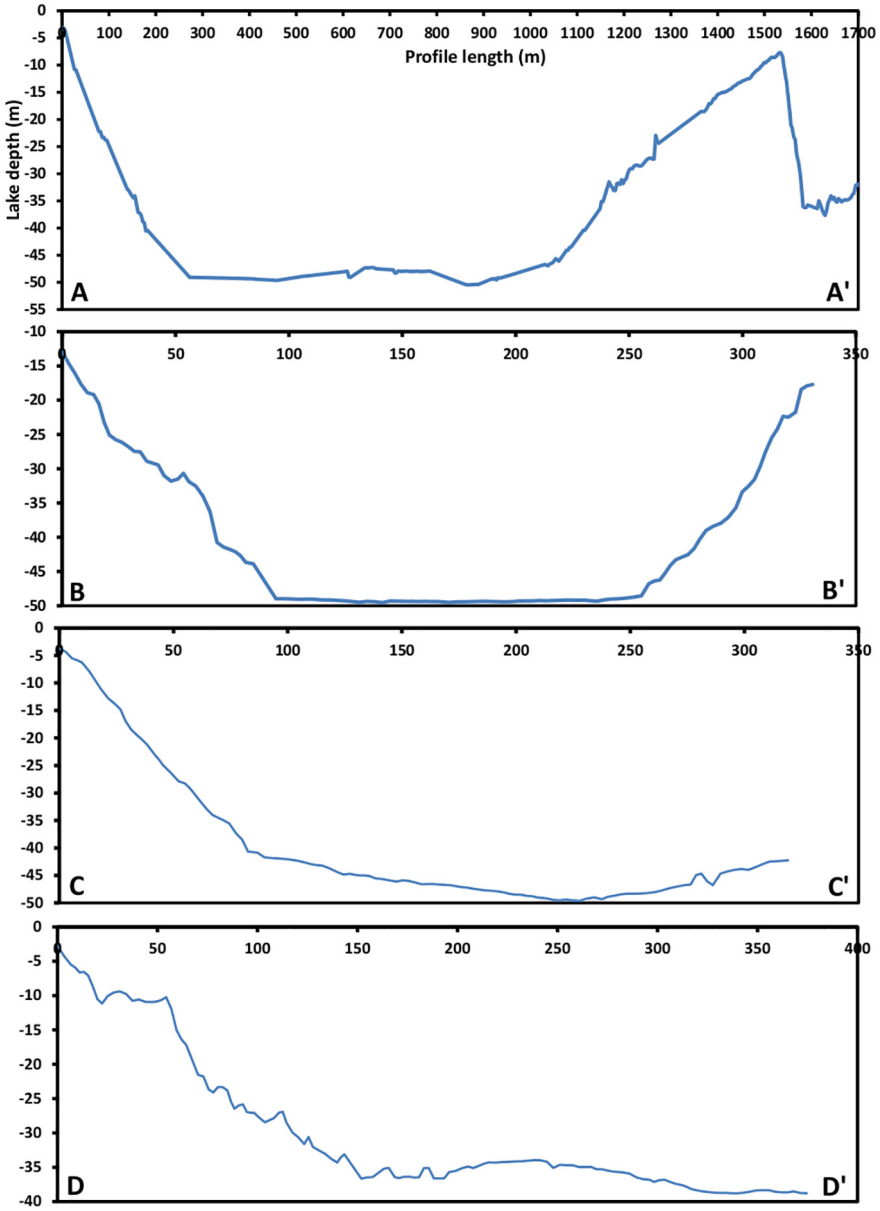

Fig. 12. Cross sections of the bathymetry survey conducted on Lake Chileno. Location of each cross section is shown on Fig. 11.

than other proglacial lakes from the region. For instance, Harrison and Winchester (2000) measured a spot depth of 103 m on Lago Arco in the Colonia Valley, whilst Warren et al. (2001) measured mean depths of 150.1 m in front of the Nef Glacier. A detailed analysis of the bathymetry of Lago Leones (Harrison et al., 2008) used 475 individual depth soundings every 100–200 m along intersecting transects across the 12-km long lake. These show that Lago Leones is over 350 m deep in places with distinct ridges rising nearly 200 m from the lake floor at 3.5, 5.5 and 7 km from the present glacier terminus. These ridges were interpreted as now-submerged moraine belts. All these lakes are moraine-dammed. Only the ice-dammed Cachet II along the flanks of the Colonia Glacier has a similarly shallow depth to Lake Chileno (averaging 49.4 m, Loriaux and Casassa, 2013). The combination of shallow depth and flat lake bed at Lake Chileno may be a consequence of significant lake infilling by debris flows and sediment-charged rivers from unstable valley sides and the glacier front. We have no data to test this assertion but large lateral moraine belts above the lake shore are currently undergoing significant erosion that is introducing moraine sediments into the lake and this process is likely to have been continuous since the Chileno Glacier receded from its LIA moraine limit in the 1870s.

5. Conclusion

Using detailed remote sensing, instrumental and geomorphological data, we have reconstructed the sequence of events and impact of the December 2015 Glacial Lake Outburst Flood (GLOF) in the Chileno Valley, Patagonia. The GLOF was probably initiated by a large debris flow into the lake from two steep and largely non-vegetated mountain gullies located northeast of the Chileno Glacier terminus. Hydrograph data suggests that the flood continued for ~7 days and 19 h with an estimated total discharge of 105.6×10^6 m^3 of water. The debris flow was deposited into the Chileno Lake causing enhanced discharge through the lake outflow and incising and redistributing lake and moraine sediments. The post-GLOF channel from the lake widened in some places by >130 m, with the surface elevation of terrain located either side of the former ravine lowering by a maximum of 38.8 ± 1.5 m. Large amounts of entrained sediment were deposited at the head of the alluvial plain as the flow reduced downstream of the LIA moraine limit and these sediments produced a ~340 m wide fan with an average increase in surface elevation over the pre-GLOF surface of 4.6 ± 1.5 m. We estimate that around 3.5 million m^3 of material was eroded from the flood-affected area whilst over 0.5 million m^3 of material was deposited in the downstream GLOF fan. The trigger mechanism for the GLOF, a large debris flow from the surrounding mountain slope, was probably a paraglacial response to glacier recession from LIA limits. We suggest that GLOFs will continue to occur in these settings in the future as glaciers further recede in response to global warming and produce potentially unstable lakes. Detailed studies of GLOF events are currently limited in Patagonia and the information presented here will therefore help to inform future glacial hazard assessments in this region.

Acknowledgements

This work was conducted as part of the 'Glacial hazards in Chile: processes, assessment, mitigation and risk management' project which is jointly funded by the UK Natural Environment Research Council (NERC) (grant NE/N020693/1) and the Chilean Natural Commission for Scientific and Technological Research (CONICYT) (grant MR/N026462/1). This work was also partly funded by the Labex DRIIHM, French programme "Investissements d'Avenir" (ANR-11-LABX-0010) which is managed by the French National Research Agency. The authors gratefully acknowledge the USGS (Landsat imagery), ESRI (WorldView-2) for free satellite data access. We would also like to thank Dr. Dana Floricioiu from the DLR for granting us access toWorldDEM data. In addition, the authors would like to thank (1) Jammie Valdivia from Colbri Ventura (Coyhaique, Chile) for providing logistical field campaign support; (2) Dr. Johnny Ryan for preparation of the fixed wing UAVs; (3) Francisco Croxatto for kindly granting us access to the Chileno Valley; (4) Dr. Jean F. Schneider for sharing his photography from a 2010 field campaign to the Chileno Valley; (5) Andres Cossio from the National Forest Corporation of Chile (CONAF) for granting us access to the Laguna San Rafael National Park; and (6) Dr. Mark Neal (Ystumtec Ltd.) for designing and building the bathymetry boat used in this study.We would also like to thank Dr. Gino Casassa for his help in the preparation of the project.

References

Augustinus, P.C., 1995. Glacial valley cross-profile development: the influence of in situ rock stress and rock mass strength, with examples from the Southern Alps, New Zealand. Geomorphology 14, 87–97.
Barcaza, G., Aniya, M., Matsumoto, T., Aoki, T., 2009. Satellite-derived equilibrium lines in Northern Patagonia Icefield, Chile, and their implications to glacier variations. Arct. Antarct. Alp. Res. 41, 174–182.
Becek, K., Koppe, W., Şenol Hakan, K., 2016. Evaluation of vertical accuracy of the WorldDEM™ using the runway method. Remote Sens. 8, 934.
Bown, F., Rivera, A., 2007. Climate changes and recent glacier behaviour in the Chilean Lake District. Glob. Planet. Chang. 59 (1–4), 79–86.
Breien, H., De Blasio, F.V., Elverhøi, A., Høeg, K., 2008. Erosion and morphology of a debris flow caused by a glacial lake outburst flood, Western Norway. Landslides 5, 271–280.
Brown, L.E, Hannah, D.M, Milner, A.M, 2006. Spatial and temporal water column and streambed temperature dynamics within an alpine catchment: implications for benthic communities. J. Hydrol 19, 1585–1610.
Carey, M., 2005. Living and dying with glaciers: people's historical vulnerability to avalanches and outburst floods in Peru. Glob. Planet. Chang. 47, 122–134.
Carrasco, J.F., Casassa, G., Rivera, A., 2002. Meteorological and climatological aspects of the Southern Patagonia Icefield. In: Casassa, G., Sepulveda, F., Sinclair, R. (Eds.), The Patagonian Icefields. A Unique Natural Laboratory for Environmental and Climate Change Studies. Kluwer Academic/Plenum Publishers, New York, pp. 29–65.
Carrivick, J.L., Quincey, D.J., 2014. Progressive increase in number and volume of ice-marginal lakes on the western margin of the Greenland Ice Sheet. Glob. Planet. Chang. 116, 156–163.
Carrivick, J.L., Tweed, F.S., 2016. A global assessment of the societal impacts of glacier outburst floods. Glob. Planet. Chang. 144, 1–16.
Cenderelli, D.A., Wohl, E.E., 2001. Peak discharge estimates of glacial-lake outburst floods and "normal" climatic floods in the Mount Everest region, Nepal. Geomorphology 40, 57–90.
Clague, J.J., Evans, S.G., 2000. A review of catastrophic drainage of moraine-dammed lakes in British Columbia. Quaternary Sci. Rev. 19, 1763–1783.
Cossart, E., Braucher, R., Fort, M., Bourlès, D.L., Carcaillet, J., 2008. Slope instability in relation to glacial debuttressing in alpine areas (Upper Durance catchment, southeastern France): evidence from field data and ^{10}Be cosmic ray exposure ages. Geomorphology 95, 3–26.
Davies, B.J., Glasser, N.F., 2012. Accelerating shrinkage of Patagonian glaciers from the Little Ice Age (~AD 1870) to 2011. J. Glaciol. 58 (212), 1063–1084.
Drusch, M., Del Bello, U., Carlier, S., Colin, O., Fernandez, V., Gascon, F., Hoersch, B., Isola, C., Laberinti, P., Martimort, P., Meygret, A., Spoto, F., Sy, O., Marchese, F., Bargellini, P., 2012. Sentinel-2: ESA's optical high-resolution mission for GMES operational services. Remote Sens. Environ. 120, 25–36.
Dussaillant, A., Benito, G., Buytaert, W., Carling, P., Meier, C., Espinoza, F., 2010. Repeated glacial-lake outburst floods in Patagonia: an increasing hazard? Nat. Hazards 54 (2), 469–481.
Emmer, A., Cochachin, A., 2013. The causes and mechanisms of moraine-dammed lake failures in the Cordillera Blanca, North American Cordillera and Himalaya. AUC. Geographica 48, 5–15.
Escobar, F., Vidal, V., Garin, C., Naruse, R., 1992. Water balance in the Patagonian icefield. In: Naruse, R. (Ed.), Glaciological Researches in Patagonia, 1990. Institute of Low Temperature Science, Hokkaido University, Sapporo, pp. 109–119.
Giese, B.S., Urizar, S.C., Fuckar, N.S., 2002. Southern Hemisphere origins of the 1976 climate shift. Geophys. Res. Lett. 29 (2), 1–4.
Glasser, N.F., Harrison, S., Jansson, K.N., 2009. Topographic controls on glacier sediment–landform associations around the temperate North Patagonian Icefield. Quat. Sci. Rev. 28 (25–26), 2817–2832.
Gruber, S., Haeberli, W., 2007. Permafrost in steep bedrock slopes and its temperature related destabilization following climate change. J. Geophys. Res. 112, F02S18.
Haeberli, W., Clague, J.J., Huggel, C., Kääb, A., 2010. Hazards from lakes in high mountain glacier and permafrost regions: climate change effects and process interactions. Avances de la Geomorphología en España, 2008–2010. XI Reunión Nacional de Geomorphología, Solsona, pp. 439–446.
Harrison, S., Winchester, V., 2000. Nineteenth-and twentieth-century glacier fluctuations and climatic implications in the Arco and Colonia valleys, Hielo Patagónico Norte, Chile. Arct. Antarct. Alp. Res. 32 (1), 55–63.
Harrison, S., Glasser, N., Winchester, V., Haresign, E., Warren, C., Jansson, K., 2006. A glacial lake outburst flood associated with recent mountain glacier retreat, Patagonian Andes. The Holocene 16 (4), 611–620.
Harrison, S., Winchester, V., Glasser, N., 2007. The timing and nature of recession of outlet glaciers of Hielo Patagónico Norte, Chile, from their Neoglacial IV (Little Ice Age) maximum positions. Glob. Planet. Chang. 59 (1–4), 67–78.
Harrison, S., Glasser, N., Winchester, V., Haresign, E., Warren, C., Duller, G.A., Bailey, R., Ivy-Ochs, S., Jansson, K., Kubik, P., 2008. Glaciar León, Chilean Patagonia: Late-Holocene chronology and geomorphology. The Holocene 18 (4), 643–652.

Harrison, S., Kargel, J.S., Huggel, C., Reynolds, J., Shugar, D.H., Betts, R.A., Emmer, A., Glasser, N., Haritashya, U.K., Klimes, J., Reinhardt, L., Schaub, Y., Wiltshire, A., Regmi, D., Vilímek, V., 2018. Climate change and the global pattern of moraine-dammed glacial lake outburst floods. Cryosphere 12, 1195–1209.
Hauser, A., 2000. Remociones en masa en Chile. Second ed. Servicio Nacional de Geología y Minería, Santiago, p. 89 Boletín No. 59. (in Spanish).
Holm, K., Bovis, M.J., Jakob, M., 2004. The landslide response of alpine basins to post-Little Ice Age glacial thinning and retreat in southwestern British Columbia. Geomorphology 57, 201–216.
Hubbard, B., Heald, A., Reynolds, J.M., Quincey, D., Richardson, S.D., Zapata Luyo, M., Santillan Portilla, N., Hambrey, M.J., 2005. Impact of a rock avalanche on a moraine-dammed proglacial lake: Laguna Safuna Alta, Cordillera Blanca, Peru. Earth Surf. Process. Landforms 30, 1251–1264.
Huggel, C., Haeberli, W., Kääb, A., Bieri, D., Richardson, S., 2004. An assessment procedure for glacial hazards in the Swiss Alps. Can. Geotech. 41, 1068–1083.
Huss, M., Bauder, A., Werder, M., Funk, M., Hock, R., 2007. Glacier-dammed lake outburst events of Gornersee, Switzerland. J. Glaciol. 53, 189–200.
Iribarren Anacona, P.I., Norton, K., Mackintosh, A., 2014. Moraine-dammed lake failures in Patagonia and assessment of outburst susceptibility in the Baker Basin. Nat. Hazards Earth Syst. Sci. 14, 3243–3259.
Iribarren Anacona, P.I., Mackintosh, A., Norton, K., 2015a. Hazardous processes and events from glacier and permafrost areas: lessons from the Chilean and Argentinean Andes. Earth Surf. Process. Landforms 40, 2–21.
Iribarren Anacona, P.I., Mackintosh, A., Norton, K., 2015b. Reconstruction of a glacial lake outburst flood (GLOF) in the Engaño Valley, Chilean Patagonia: lessons for GLOF risk management. Sci. Total Environ. 527–528, 1–11.
Iturrieta, F., 2017. Mudslide in southern Chile kills five, at least 15 missing. [online] Available at: https://www.reuters.com/article/us-chile-landslide/mudslide-in-southern-chile-kills-five-at-least-15-missing-idUSKBN1EA0PG (Accessed 10 Jan. 2018).
Kääb, A., Reynolds, J.M., Haeberli, W., 2005. Glacier and permafrost hazards in high mountains. In: Huber, U.M., Bugmann, H.K.M., Reasoner, M.A. (Eds.), Global Change and Mountain Regions (A State of Knowledge Overview). Springer, Dordrecht, pp. 225–234.
Keiler, M.K., Knight, J., Harrison, S., 2010. Climate change and geomorphological hazards in the eastern European Alps. Phil. Trans. R. Soc. A 368, 2461–2479.
Kershaw, J.A., Clague, J.J., Evans, G., 2005. Geomorphic and sedimentological signature of a two-phase outburst flood from moraine-dammed Queen Bess Lake, British Columbia, Canada. Earth Surf. Process. Landforms 30, 1–25.
Loriaux, T., Casassa, G., 2013. Evolution of glacial lakes from the Northern Patagonia Icefield and terrestrial water storage in a sea-level rise context. Glob. Planet. Chang. 102, 33–40.
Lumbroso, D., Gaume, E., 2012. Reducing the uncertainty in indirect estimates of extreme flash flood discharges. J. Hydrol. 414-415, 16–30.
Masiokas, M.H., Villalba, R., Luckman, B.H., Lascano, M.E., Delgado, S., Stepanek, P., 2008. 20th-century glacier recession and regional hydroclimatic changes in northwestern Patagonia. Glob. Planet. Chang. 60, 85–100.
Matsuoka, K., Naruse, R., 1999. Mass balance features derived from a firn core at Hielo Patagonico Norte, South America. Arct. Antarct. Alp. Res. 31, 333–340.
Montecinos, A., Aceituno, P., 2003. Seasonality of the ENSO related rainfall variability in Central Chile and associated circulation anomalies. J. Clim. 16 (2), 281–296.
Nie, Y., Liu, Q., Liu, S., 2013. Glacial lake expansion in the Central Himalayas by Landsat Images. PLoS One 8, e83973.
Nie, Y., Sheng, Y.W., Liu, Q., Liu, L.S., Liu, S.Y., Zhang, Y.L., Song, C.Q., 2017. A regional-scale assessment of Himalayan glacial lake changes using satellite observations from 1990 to 2015. Remote Sens. Environ. 189, 1–13.
Nie, Y., Liu, Q., Wang, J., Zhang, Y., Sheng, Y., Liu, S., 2018. An inventory of historical glacial lake outburst floods in the Himalayas based on remote sensing observations and geomorphological analysis. Geomorphology 308, 91–106.
Osti, R., Egashira, S., 2009. Hydrodynamic characteristics of the Tam Pokhari Glacial Lake outburst flood in the Mt. Everest region, Nepal. Hydrol. Process. 23, 2943–2955.
Paul, F., Mölg, N., 2014. Hasty retreat of glaciers in northern Patagonia from 1985 to 2011. J. Glaciol. 60 (244), 1033–1043.
Paul, F., Kääb, A., Haeberli, W., 2007. Recent glacier changes in the Alps observed by satellite: consequences for future monitoring strategies. Glob. Planet. Chang. 56, 111–122.
Rasmussen, L.A., Conway, H., Raymond, C.F., 2007. Influence of upper air conditions on the Patagonia icefields. Glob. Planet. Chang. 59, 203–216.
Reynolds, J.M., 1992. The identification and mitigation of glacier-related hazards: examples from the Cordillera Blanca, Peru. In: McCall, G.J.H., Laming, D.J.C., Scott, S.C. (Eds.), Geohazards. Chapman & Hall, London, pp. 143–157.
Reynolds, J.M., 2014. Assessing glacial hazards for hydro development in the Himalayas, Hindu Kush and Karakorum. International Journal of Hydropower and Dams 2, 60–65.
Richardson, S.D., Reynolds, J.M., 2000. An overview of glacial hazards in the Himalayas. Quat. Int. 65/66 (1), 31–47.
Riegler, G., Hennig, S.D., Weber, M., 2015. WORLDDEM - a novel global foundation layer, ISPRS—Int. Arch. Photogramm. Remote. Sens. Spat. Inf. Sci. XL-3-W2 183–7.
Rounce, D.R., McKinney, D.C., Lala, J.M., Byers, A.C., Watson, S., 2016. A new remote hazard and risk assessment framework for glacial lakes in the Nepal Himalaya. Hydrol. Earth Syst. Sci. 20, 3455–3475.
Ryan, J.C., Hubbard, A.L., Box, J.E., Todd, J., Christoffersen, P., Carr, J.R., Holt, T.O., Snooke, N., 2015. UAV photogrammetry and structure from motion to assess calving dynamics at Store Glacier, a large outlet draining the Greenland ice sheet. Cryosphere 9, 1–11.
Taylor, J.R., 1982. An Introduction to Error Analysis. Oxford Univ. Press, Oxford.
Ullman, S., 1979. The interpretation of structure from motion. P. R. Soc. London 203 (405–426), 1979.
UNEP, 2007. Global Outlook for Ice and Snow. UNEP, (235 p).
Villalba, R., Masiokas, M., Kitzberger, T., Boninsegna, J.A., 2005. Biogeographical consequences of recent climate changes in the southern Andes of Argentina. In: Huber, U.M., Bugmann, H.K.M., Reasoner, M.A. (Eds.), Global Change and Mountain Regions, an Overview of Current Knowledge. Springer, Switzerland, pp. 157–166.
Vuichard, D., Zimmermann, M., 1987. The 1985 catastrophic drainage of a moraine-dammed lake, Khumbu Himal, Nepal: cause and consequences. Mt. Res. Dev. 7 (2), 91–110.
Wang, W., Xiang, Y., Gao, Y., Lu, A., Yao, T., 2014. Rapid expansion of glacial lakes caused by climate and glacier retreat in the central Himalayas. Hydrol. Process. 29, 859–874.
Warren, C., Benn, D., Winchester, V., Harrison, S., 2001. Buoyancy-driven lacustrine calving, Glaciar Nef, Chilean Patagonia. J. Glaciol. 47 (156), 135–146.
Webb, R.H., Jarrett, R.D., 2002. One-dimensional estimation techniques for discharges of paleofloods and historical floods. In: House, P.K., Webb, R.H., Baker, V.R., Levish, D.R. (Eds.), Ancient Floods, Modern Hazards, Principles and Applications of Paleoflood Hydrology. American Geophysical Union Water Science and Application Series 5, pp. 111–125.
Westoby, M.J., Brasington, J., Glasser, N.F., Hambrey, M.J., Reynolds, J.M., 2012. 'Structure-from-Motion' photogrammetry: a low-cost, effective tool for geoscience applications. Geomorphology 179, 300–314.
Westoby, M.J., Glasser, N.F., Hambrey, M.J., Brasington, J., Mohamed, M.A.A.M., 2014a. Reconstructing historic Glacial Lake Outburst Floods through numerical modelling and geomorphological assessment: extreme events in the Himalaya. Earth Surf. Proc. Land. 39, 1675–1692.
Westoby, M.J., Glasser, N.F., Brasington, J., Hambrey, M.J., Quincey, D.J., Reynolds, J.M., 2014b. Modelling outburst floods from moraine-dammed glacial lakes. Earth-Sci. Rev. 134, 137–159.
Wilson, R., Glasser, N.F., Reynolds, J.M., Harrison, S., Iribarren Anacona, P., Schaefer, M., Shannon, S., 2018. Glacial lakes of the central and Patagonian Andes. Global Plant. Change 162, 275–291.
Worni, R., Stoffel, M., Huggel, C., Volz, C., Casteller, A., Luckman, B., 2012. Analysis and dynamic modeling of a moraine failure and glacier lake outburst flood at Ventisquero Negro, Patagonian Andes (Argentina). J. Hydrol. 444-445, 134–145.